Int J Adv Manuf Technol (2017) 88:1821–1830
DOI 10.1007/s00170-016-8929-1

ORIGINAL ARTICLE

Understanding and elimination of process defects in narrow gap multi-pass fiber laser welding of ferritic steel sheets of 30 mm thickness

Jiecai Feng[1] · **Wei Guo**[1] · **Neil Irvine**[1] · **Lin Li**[1]

Received: 18 December 2015 / Accepted: 12 May 2016 / Published online: 24 May 2016

Abstract Narrow gap (or groove) laser welding involves multiple layer additive manufacture for the joining of thick-section metallic components. Typical defects include porosity, cracking, lack of fusion to sidewalls, and between layers, and component distortion including the closure of the groove. This study aimed to understand the defect formation mechanisms and factors affecting them, and to develop appropriate welding procedures and parameters for joining ferritic steel sheets of 30 mm in thickness. High-quality welded joints in 30-mm-thick Grade 43 ferritic steel sheets have been achieved by multi-pass defocused laser beam welding with filler wire addition. The microstructure and the microhardness of the multi-pass welded joint were found to be affected by the tempering of the subsequent multi-pass welding layers. Post-weld heat treatment on the welded joints were required since, although the strength of the welded joints were higher than that of base metal, the ductility was much lower than that of base metal.

Keywords Narrow gap · Multi-pass · Laser welding · Thick-section · Ferritic steel

✉ Jiecai Feng
fengjc@sh-lslaser.com; fjc2002@sina.com

[1] Laser Processing Research Centre, School of Mechanical, Aerospace and Civil Engineering, The University of Manchester, Manchester M13 9PL, UK

1 Introduction

Pressurized water reactor (PWR) pressure vessels are of a cylindrical shell design, 3.3~4.6 m in diameter and 12~14 m in height, with a through-wall thickness of about 230 mm [1]. The primary welding technology for the nuclear pressure vessel manufacture is multi-pass submerged arc welding (SAW) [2, 3]. However, compared with the electron beam welding (EBW) and laser beam welding (LBW), SAW generally employs a high heat input, resulting in large distortions and residual stresses after welding. Additionally, a relatively wide V-shape groove is commonly used in SAW, which means that large number of weld passes and large amount of filler material are required. For instance, a heat input of 1.8 kJ/mm and a ~50-mm wide groove are required for welding SA533 and SA508 steel plates of 140 mm thickness using multi-pass SAW [3]. Using EBW for joining thick-section pressure vessels and pipes, a 160-mm-thick SA508 steel component has been welded using a reduced pressure electron beam single-pass welding process [4]. LBW is more flexible as a laser beam can be transmitted by optical fibers, which makes laser welding amenable to the manufacture of complex components [5–9]. Jones et al. [10] demonstrated that with a groove width of only 6 mm, excellent quality welds in a 60-mm thick-walled stainless steel tube were produced by narrow gap multi-pass laser welding with filler wire addition. Compared with arc welding, the heat input decreased from 2.5 to 1.1 kJ/mm and the number of welding passes also was reduced from 30 to 13. Zhang et al. [11] reported that with 8 passes, butt joining of 50-mm-thick stainless steel plates could be achieved by multi-pass narrow gap laser welding with filler wire addition. Recently,

Table 1 Chemical composition of the Grade 43 ferritic steel and filler wire (wt.%)

	C	Si	Mn	P	S	Cr	Ni	Mo	Cu
Steel	0.14	0.04	0.85	0.016	0.01	0.014	0.011	0.001	0.008
Wire	0.10	0.20	1.14	0.006	0.005	0.03	0.88	0.25	0.075

Elmesalamy et al. [12] reported that compared with arc welding, the number of weld passes for narrow gap laser welding with filler wire addition decreased from 43 to 20, when welding 20-mm-thick AISI grade 316 L stainless steel plates. It is generally accepted that compared with SAW, the EBW and LBW techniques offer higher welding speeds, lower levels of residual stress and distortion, while consuming less filler material [13–17].

Most previous investigations in laser narrow gap welding were focused on the thick-section stainless steels. Little attention has been devoted to the ferritic steels. Compared with stainless steels, ferritic steels have higher specific heat, higher coefficient of thermal conductivity (~3 times of that of stainless steel), which means that narrow gap laser welding for ferritic steels has a higher risk of leading to the lack of sidewall fusion than for stainless steels. In this paper, we report narrow gap multi-pass laser welding with filler wire addition of a 30-mm-thick Grade 43 ferritic steel. The research focus was placed on the understanding of defect formation. The welding procedures were optimized to eliminate defects such as cracking, lack of fusion and porosity. Additionally, the microstructures and mechanical properties evolution of the multi-pass welded joint were analyzed in detail.

2 Experimental procedure

The materials used in the study were Grade 43 ferritic steel with dimensions of 300 mm (length) × 135 mm (width) × 30 mm (thickness) and a filler wire with a diameter of 1.2 mm. Their chemical compositions are listed in Table 1.

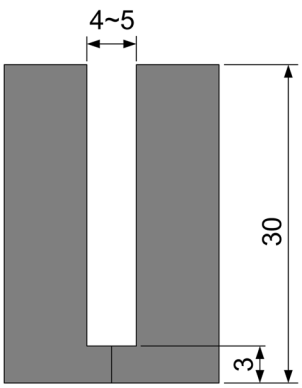

Fig. 1 Schematic representation of groove shape (units in mm)

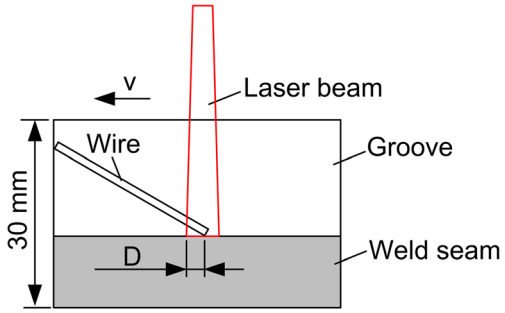

Fig. 2 Schematic representation of narrow gap multi-pass laser welding process with filler wire addition

Ar gas with an 8 l/min flow rate was used as the shielding gas. A butt joint configuration with a 4 to 5 mm width square groove was prepared as shown in Fig. 1. A schematic representation of the narrow gap multi-pass laser welding process with filler wire addition is shown in Fig. 2, where *D* is the distance between the edge of the laser spot to the tip of the wire, and is defined as the laser-wire overlapping. The shielding gas was delivered with a 3-mm diameter tube inside the weld groove of the narrow gap multi-pass laser welding process with filler wire addition in the first method (Fig. 3), while in the second method, the shielding gas was delivered by a 15-mm-diameter tube on the top of the weld groove (Fig. 4). The specimen surfaces were cleaned with acetone before welding to eliminate surface contamination.

The welding system consisted of an IPG (YLS-16000) continuous wave (CW) solid-state ytterbium fiber laser system with a maximum power of 16 kW and an Arc Welding Products (F4) wire feeder. This was mounted on a six-axis KUKA welding robot. The beam parameter product of the laser was 10 mm·mrad and the diameter of the beam delivery fiber was 300 μm. The collimation length was 150 mm and the focal length for the focusing lens was 400 mm. The diameter of the

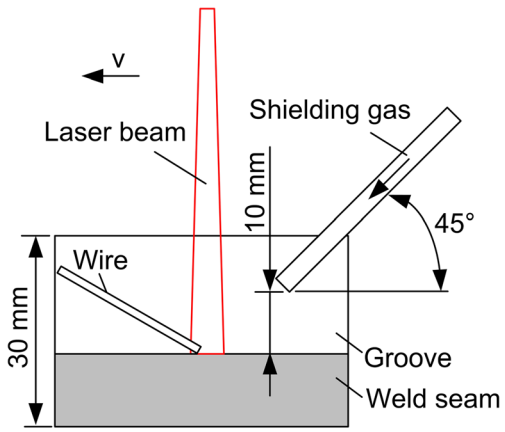

Fig. 3 Schematic representation of shielding gas method with a small diameter tube

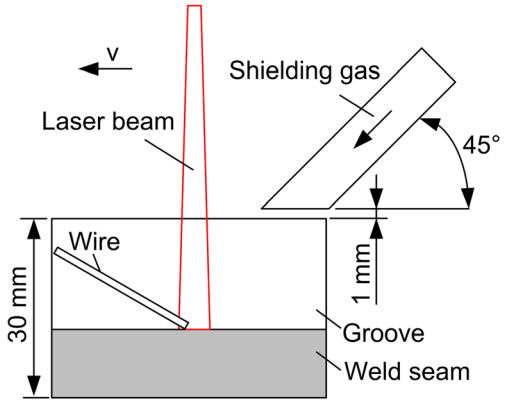

Fig. 4 Schematic representation of shielding gas method with a large diameter tube

laser spot was 6 mm on the target surface. The various laser heat input investigated ranged from 0.9 to 1.2 kJ/mm. The laser-wire over lapping was varied from 1 to 5 mm. The wire feed rate was varied from 4 to 6 m/min. The various welding velocities ranged from 0.3 to 0.5 m/min.

The welded specimen cross-sections were polished and etched using a solution of a mixture of 5 ml nitric acid and 95 ml ethanol. Microscopic examination was carried out using a KEYENCE VHX-500 F optical microscope and a Hitachi S3000N model scanning electron microscope (SEM). Microhardness of the welded joint was measured using an automatic Vickers microhardness machine with a load of 3 kg and a dwell period of 10 s.

Full-size transverse tensile specimens with and without notch were machined from the welded joint (Fig. 5a, c), for tensile strength testing, on a WE-1000B tensile machine with 1 mm/min crossbeam velocity at 20 °C. The depth and the width of the notch are 10 mm and 0.5 mm, respectively. In addition, as shown in Fig. 5b, longitudinal tensile specimens were specially designed for the tensile tests at 20 °C. The longitudinal tensile specimens were cut into dimensions of 50 mm × 8 mm × 1.5 mm (Fig. 5d), and the tensile tests were carried out on an Instron-5500R tensile machine with 0.5 mm/min crossbeam velocity at 20 °C. It should be emphasized that the longitudinal tensile specimens consisted of the weld zone (i.e. primarily the filler wire) only. The base metal specimens with the same dimensions were also tested for comparison.

3 Results and discussion

3.1 Factors affecting the welding quality

3.1.1 Effect of laser heat input on crack formation

The cross-sectional weld bead profiles for welded joints with different laser heat input are shown in Fig. 6. It can be seen that there were 2.3 mm deep longitudinal surface cracks in the welded joint when the laser heat input was 0.9 kJ/mm (Fig. 6a). However, when the heat input increased to 1.05 kJ/mm, the length of the longitudinal surface cracks decreased to 0.8 mm. A welded joint without cracks was achieved when the laser heat input reached 1.2 kJ/mm (Fig. 6b). This is because that laser welding is associated with relatively high cooling rates, which results in increased risks for cracking when compared with arc welding techniques. With a higher

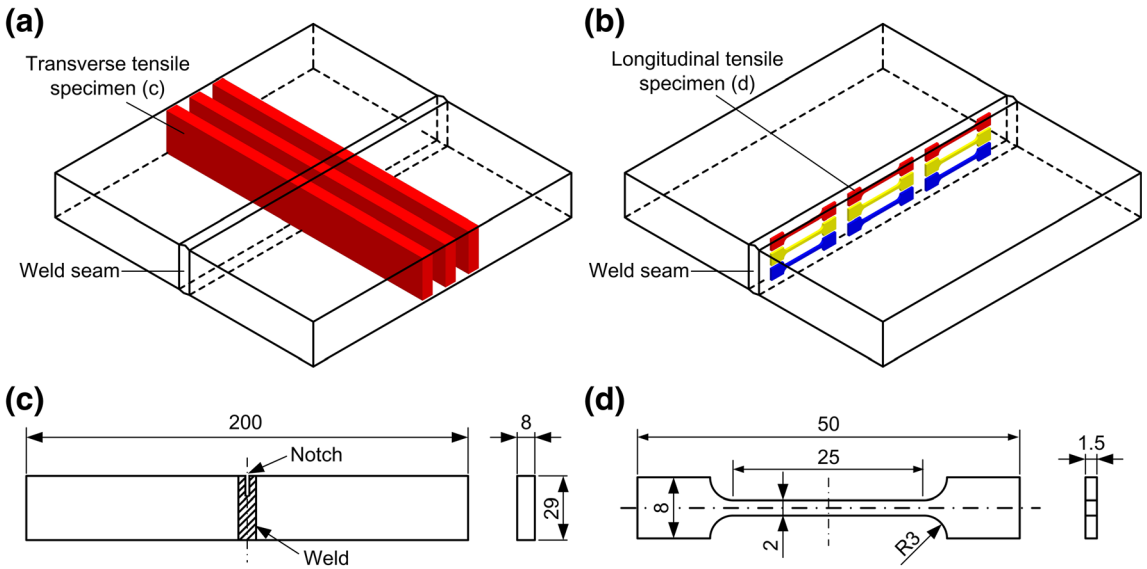

Fig. 5 Schematic of sampling location: **a** transverse tensile specimens, **b** longitudinal tensile specimens, dimensions of: **c** transverse tensile specimen and **d** longitudinal tensile specimen

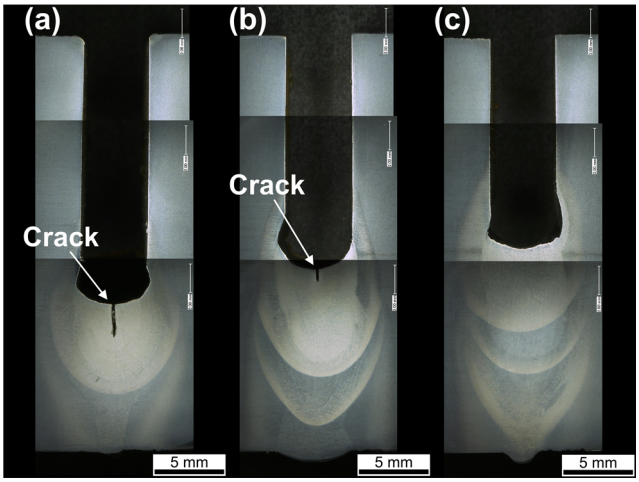

Fig. 6 Effect of the laser heat input on multi-pass laser welding with filler wire addition: **a** 0.9 kJ/mm, **b** 1.05 kJ/mm, and **c** 1.2 kJ/mm

laser heat input the cooling rate of the weld pool could be reduced resulting in fewer risks for cracking.

3.1.2 Effect of laser-wire overlapping on side wall fusion and spatter

Figure 7 shows the cross sectional weld bead profiles for welded joints with different laser-wire overlapping. It can be seen that when the overlapping was 1 mm, the welded joint without lack of sidewall fusion and spatters was obtained. However, when the overlapping was 3 mm, lack of sidewall fusion (arrow) was formed in the welded joint. For the overlapping of 5 mm, overlap (circle) was formed on the sidewall of the welded groove. This is because that molten metal was formed on the tip of the feeding wire by absorbing part of the laser energy. When the overlapping was 1 mm, the molten metal contacted with the weld pool and it was transferred to the weld pool and spread. However, when the overlapping

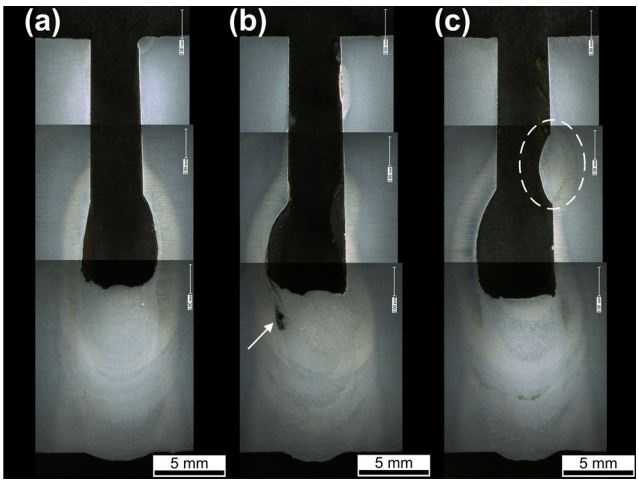

Fig. 7 Effect of the laser-wire overlapping on multi-pass laser welding with filler wire addition: **a** 1 mm, **b** 3 mm, and **c** 5 mm

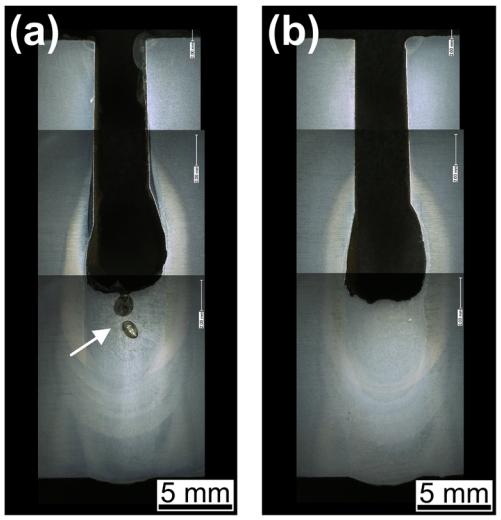

Fig. 8 Effect of the shielding gas method on multi-pass laser welding with filler wire addition: **a** 5 mm diameter tube inside groove and **b** 15 mm diameter tube on the top of the groove

was 3 mm, the molten metal did not contact with the weld pool and it could not be transferred to the weld pool directly, while it dropped to the weld pool, which would cause lack of sidewall fusion. When the overlapping increased to 5 mm, spatter was found on the sidewall of the groove by the molten metal as the molten metal on the tip of the wire was far away from the weld pool, resulting in less deposited metal on the welded joint.

3.1.3 Effect of shielding gas method on porosity formation

The weld bead profiles for welded joints with different shielding gas method are shown in Fig. 8. It can be seen that there was large-scale porosity (arrow) in the welded joint when the shielding gas was delivered by a 3-mm diameter tube inside the weld groove (Fig. 8a). However, when the shielding gas was delivered by a 15-mm diameter tube on the top of the weld groove, a welded joint without porosity was achieved (Fig. 8b). This is because that the shielding gas flow velocity

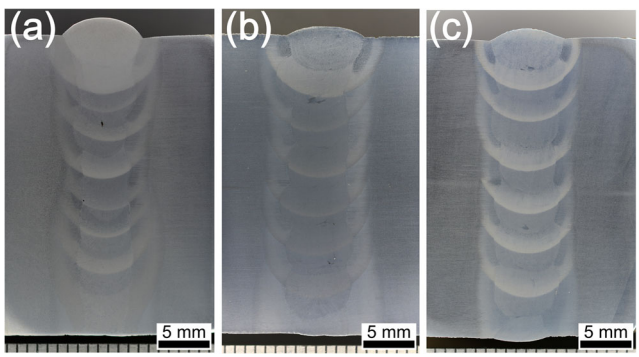

Fig. 9 Effect of the feed rate of wire on multi-pass laser welding with filler wire addition: **a** 4 m/min, **b** 5 m/min and, **c** 6 m/min

was too high when the diameter of the tube was too small, creating turbulence. When the shielding gas flowed very gently from the top of the weld groove, the weld groove was filled with shielding gas, which can prevent oxygen and air coming into the weld pool.

3.1.4 Effect of the feeding rate of wire on welding efficiency

The weld bead profiles for welded joints with different feed rates for the filler wire are shown in Fig. 9. It can be seen that when the feed rate of the wire increased from 4 to 6 m/min, the number of weld passes decreased from 12 to 8. This is because the depth for each filling pass in the welded joint increases when the feed rate of the wire increases.

The optimized laser welding parameters are: laser heat input 1.2 kJ/mm, laser-wire over lapping 1 mm, shielding gas fed from the top of the weld groove by 15 mm diameter tube in flow rate of 15 l/min, wire feed rate 5 to 6 m/min and welding speed 0.3 to 0.4 m/min.

3.2 X-ray non-destructive inspection

The welds were examined by an engineering inspection and consultancy service company (RSA), who are qualified to assess welds to ASME IX QW 191: 2013 requirements. Their X-ray non-destructive inspection report stated that the welds were found to comply with the acceptance ASME IX standard with no lack of sidewall fusion, but some limited and acceptable porosity. The X-ray film is shown in Fig. 10.

3.3 Mechanical properties and fracture characteristics

Two different types of specimens were prepared for the tensile testing. One type is with a notch in the fusion zone to show the strengths of the welded area. The other type is without a notch to mainly show the fractures on the base metal. Figure 11 demonstrates the stress-strain relation curves of transverse tensile specimens of welded joints with and without notch in the weld metal. The figure shows that the fractures occurred in the base metal in the welded specimens without notch. For the 8 passes welded joint with a notch in the weld zone, the yield strength (YS) and ultimate tensile strength (UTS) were 490 and 580 MPa, respectively, which are higher than those of 8 passes welded joint without notch having a YS of 350 MPa and a

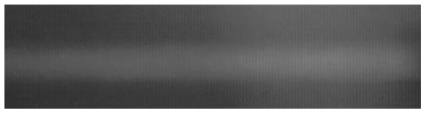

Fig. 10 X-ray non-destructive inspection film

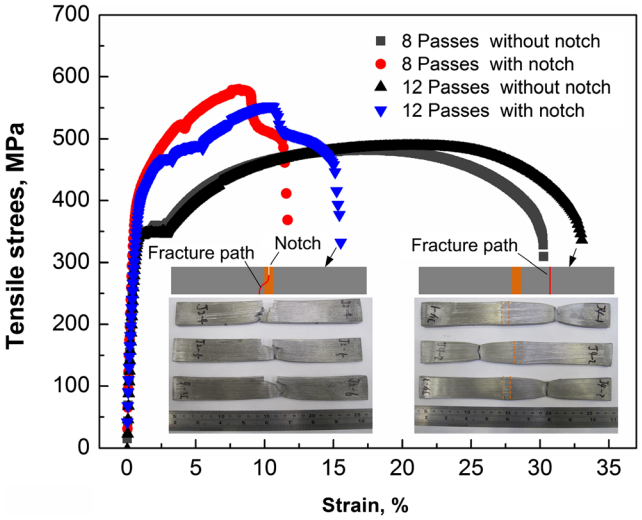

Fig. 11 Stress-strain relationship of transverse tensile specimens of welded joint with and without notch

UTS of 490 MPa. For the 12 passes welded joint with a notch, the YS and UTS are 480 and 550 MPa, respectively, which are higher than those of 12 passes welded joint without a notch having a YS of 350 MPa and a UTS of 500 MPa. On the contrary, ductilities of the welded joints with a notch are lower than that of welded joints without notch.

As the fracture morphology reflects the strength and ductility of tensile specimen, the representative fractographs of welded joint with and without a notch were analyzed, as shown in Figs. 12 and 13, respectively. Figure 12 shows the fracture path in the welded specimens with a notch: the crack grows in the weld metal first and then propagates into the base metal (Fig. 12a–c). Dimples and micro-voids are shown on the fracture surface of the weld metal and the base metal, which indicates that the specimens failed in a characteristic ductile fracture. This is because that the ferrite-carbide microstructure of base metal fails in a ductile mode with dimples initiated by granular carbides, and that the martensite having a sufficient mobility of dislocations in the weld metal can also fracture in ductile dimple mode. However, the sizes of the dimples are significantly different in these zones. As shown in Fig. 12d, small equiaxed dimples are shown on the fracture surfaces of weld metal. In contrast, large dimples are usually linked by several smaller dimples on the fracture surface of base metal, as shown in Fig. 12e. Figure 13 also shows that large dimples are linked by several smaller dimples on the fracture surface of the welded joint without a notch. Some researchers reported that large dimples observed on the fracture surface were consistent with reasonably high ductility, while small equiaxed dimples were consistent with high

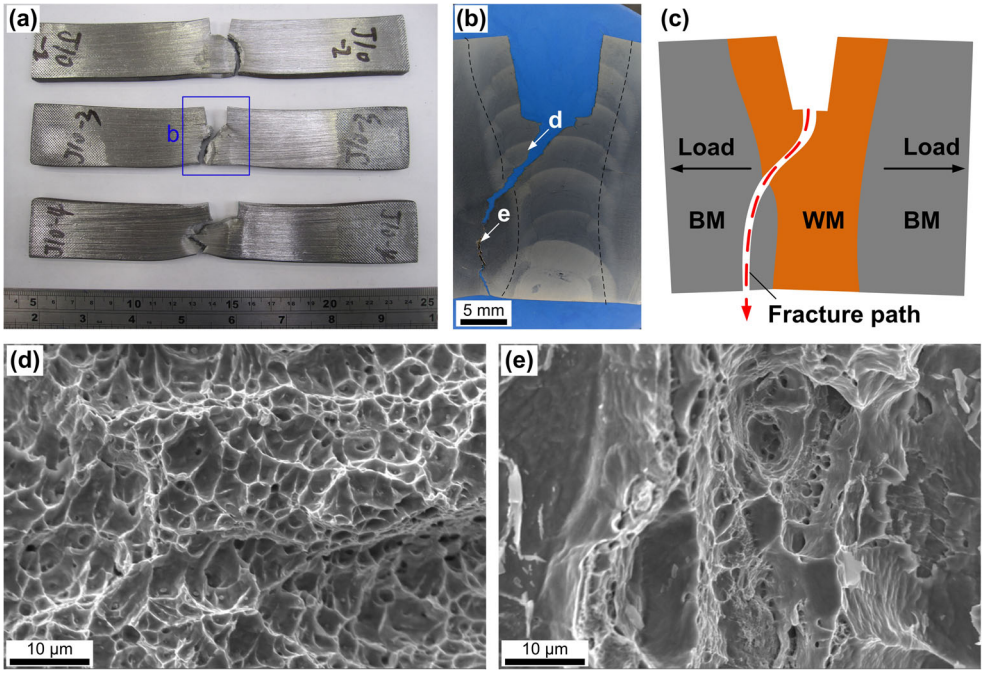

Fig. 12 Fracture path and morphology of transverse tensile specimens of welded joint with notch

strength [18, 19]. Therefore, the strengths of welded joint with a notch increase, while the ductilities decrease compared with welded joint without a notch, which are consistent with the results obtained in the tensile tests.

Longitudinal weld metal tensile specimens were compared to those of base metal as for common transverse tensile specimen, fractures occurred in the base metal instead of the weld metal, as shown in Fig. 14. J1, J2, and J3 are 8 passes welded joints with laser power of 7, 6.5, and 6 kW and with constant welding speed of 0.3 m/min, wire feed rate of 6 m/min. The figure shows that the YS and UTS of welded joint with laser power of 7 kW are about 590 and 640 MPa, respectively (Fig. 14b), while the YS and UTS of welded joint with laser power of 6.5 kW are about 630 and 700 MPa, respectively (Fig. 14c). Additionally, the YS and UTS of welded joint with a laser power of 6 kW were about 710 and 800 MPa, respectively (Fig. 14d), which are higher than those of base metal having a YS of 350 MPa and a UTS of 490 MPa (Fig. 14a). The classic Hall-Petch relationship has been used to describe the relationship between the yield stress and grain size, through the expression

$$\sigma_y = \sigma_0 + k_y d^{-1/2} \tag{1}$$

where σ_y is the yield stress, σ_0 is the friction stress needed to move individual dislocations, k_y is a positive constant of yielding associated with the stress required to extend dislocation activity into adjacent unyielded grains, and d is the average grain size [20, 21]. This relationship demonstrates that the yield strength of welded joint with smaller grain sizes is higher.

The stress-strain relation curves also show that the ductilities of the welded joints are lower than that of base metal, which means that post-weld heat treatment on the welded joints are required to reduce the strength of the welded joint while to increase the ductilities of the welded joints.

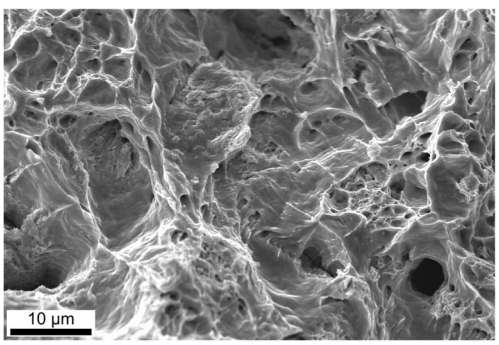

Fig. 13 Representative fractograph of welded joint without a notch

3.4 Microhardness

Figure 15 shows the microhardness contour map of a 12 passes welded joint. The figure shows that the average microhardness of the BM was 150 HV. The maximum microhardness (~310 HV) was located in the HAZ of the last welding pass, while the microhardness in the HAZ of the other welding passes was about 240 HV. The minimum microhardness on the FZ was located at the bottom of the welded joint. The diminution of the microhardness in the HAZ and the FZ means that subsequent multi-pass welding have a significant heat

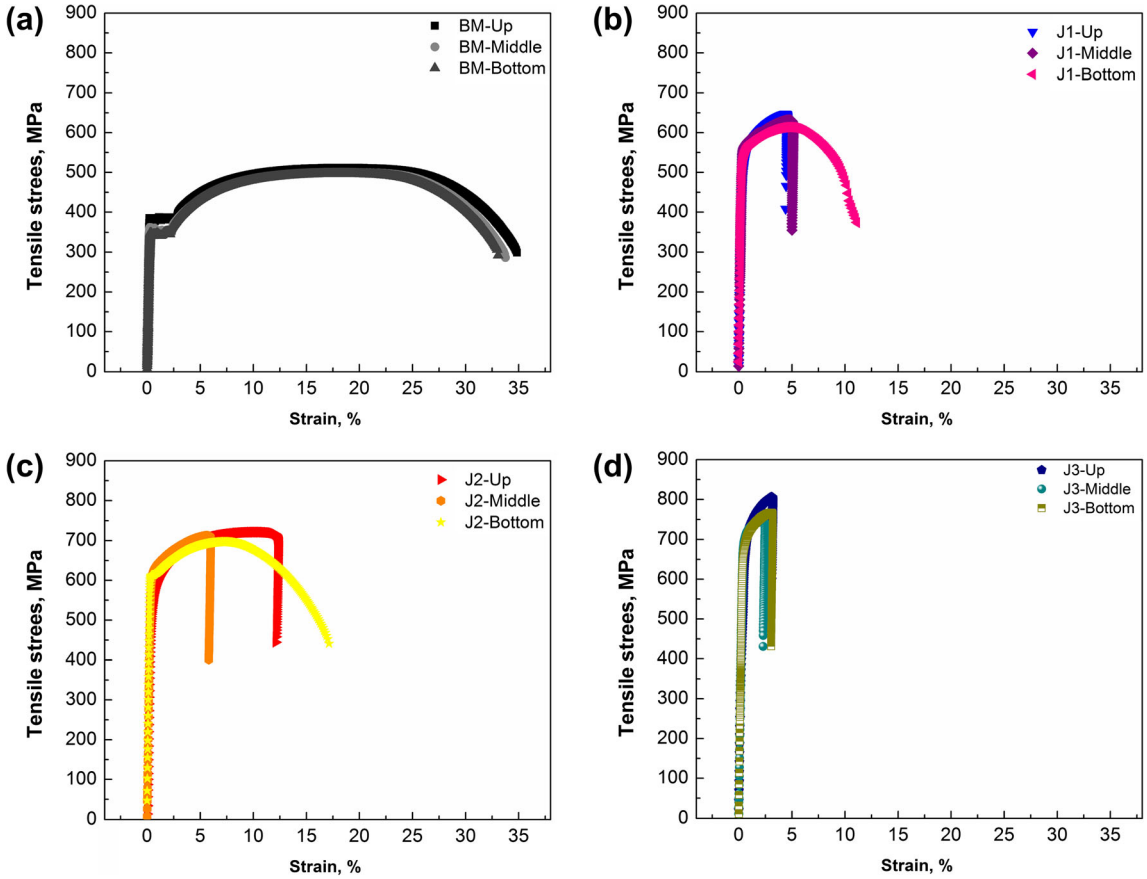

Fig. 14 Stress-strain relationship of longitudinal weld metal and base metal tensile specimens

treatment effect on the previous welding passes. The average microhardness of the HAZ in the last pass was maximum because it was the final filling pass and so there was no tempering effect on it associated with subsequent welding passes.

3.5 Microstructure

Figures 16, 17 and 18 show the weld bead profiles and the microstructures of the 1st pass, 6th pass and the 13th pass in the welded joint with multi-pass welding. It can be seen that in the 1st pass, the microstructure in the ICHAZ is composed of ferrite and tempered martensite (Fig. 16a). The microstructures in the FGHAZ, CGHAZ, and FZ are composed of tempered martensite (Fig. 16b, c, and d). For the 6th pass, the microstructure in the ICHAZ is also composed of ferrite and tempered martensite (Fig. 17a). The microstructures in the FGHAZ and CGHAZ consist of tempered martensite (Fig. 17b and c), but the martensites are not significantly decomposed into ferrite and carbides when compared with those in the 1st pass. The microstructure in the FZ

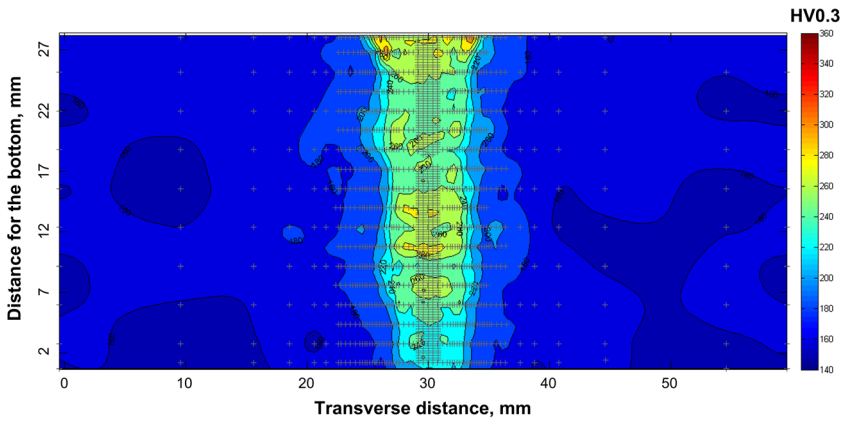

Fig. 15 Microhardness 2D contour map of a welded joint

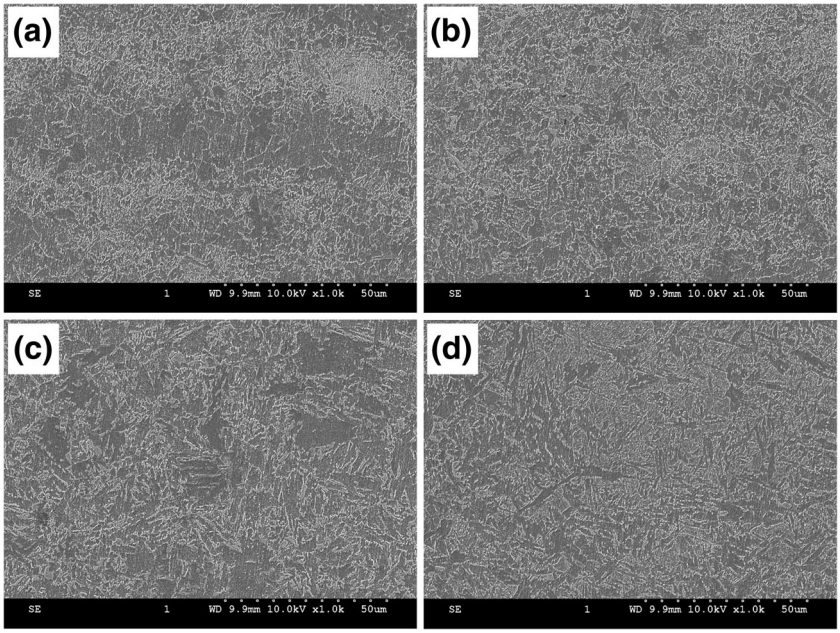

Fig. 16 Microstructure of first pass: **a** ICHAZ, **b** FGHAZ, **c** CGHAZ, and **d** FZ

includes bainite, martensite, tempered bainite and tempered martensite due to the effect of the filling wire and the tempering treatment of the subsequent multi-pass welding (Fig. 17d). For the 13th pass, the microstructure in the ICHAZ is composed of ferrite and martensite (Fig. 18a). The microstructures in the FGHAZ and CGHAZ consisted of martensite (Fig. 18b and c). The microstructure in the FZ mainly consists of bainite and martensite (Fig. 18d). Consequently, the microhardness in the HAZ of the 13th pass (last pass) is at a maximum when compared with the 1st and 6th pass due to the martensitic microstructure in the HAZ of 13th pass.

4 Conclusions

In this paper, multi-pass narrow gap laser welding with filling wire was developed for joining Grade 43 ferritic steel of 30 mm thickness. The following conclusions were drawn:

(1) Cracking, lack of sidewall fusion and porosity are the main potential defects in the multiple-pass narrow gap laser welding of thick-section ferritic steel, and these defects can be eliminated with appropriate welding procedures and parameters. Laser heat input can be used to control cracking. Laser beam and wire overlapping can

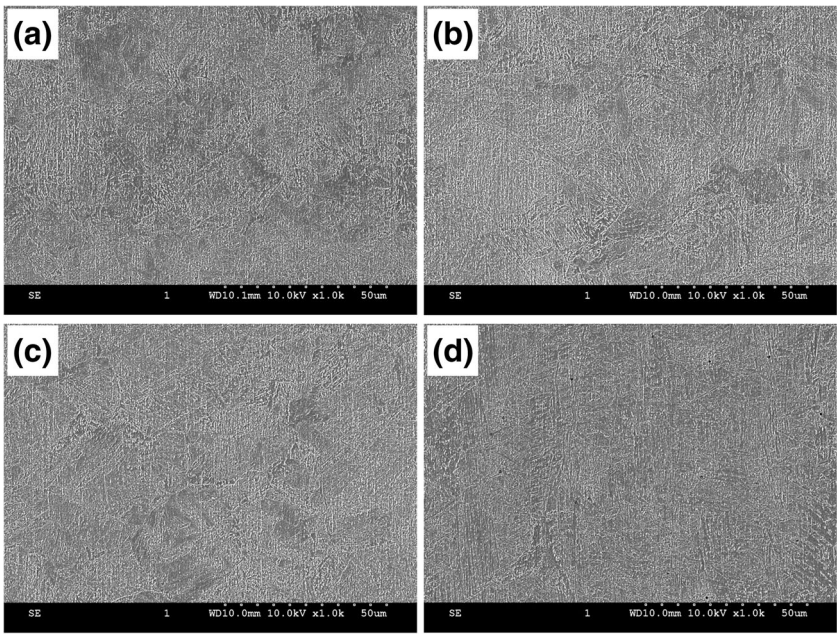

Fig. 17 Microstructure of 6th pass: **a** ICHAZ, **b** FGHAZ, **c** CGHAZ, and **d** FZ

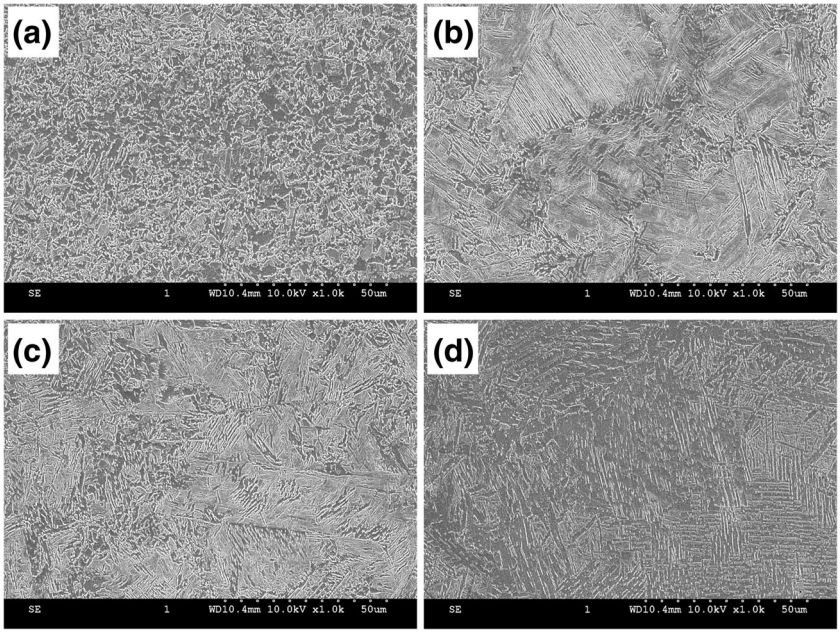

Fig. 18 Microstructure of 13th pass: **a** ICHAZ, **b** FGHAZ, **c** CGHAZ, and **d** FZ

be sued to control sidewall fusion. Slow and gently shielding gas can be used to control porosity. High quality welded joints in 30-mm-thick Grade 43 ferritic steel have been achieved by multi-pass defocused laser welding with filler wire addition.

(2) Post-weld heat treatment on the welded joints is recommended as the strength of the weld metal was much higher than that of base metal, while the ductility was lower than that of base metal.

(3) The microhardness in the HAZ and FZ in the multi-pass welding varies with the final pass having the highest hardness, due to the tempering of subsequent welding passes.

(4) In the multi-pass welded joints, the microstructure in the ICHAZ was composed of ferrite and tempered martensite. The microstructures in the FGHAZ, CGHAZ, and FZ were composed of bainite, martensite, tempered bainite and tempered martensite due to the effect of the filling wire and the tempering treatment of the subsequent multi-pass welding.

Acknowledgments The authors gratefully acknowledge financial support provide by the Engineering and Physical Sciences Research Council in the NNUMAN (New Nuclear Manufacturing) program (Grant number: EP/J021172/1).

References

1. Murtya KL, Miraglia PQ, Mathew MD, Shah VN, Haggag FM (1999) Characterization of gradients in mechanical properties of SA-533B steel welds using ball indentation. Int J Press Vessel Pip 76:361–369
2. Zhang XP, Dorn L (1999) Investigation on the possibility of using the microshear test as a surveillance method to estimate the mechanical properties and fracture toughness of nuclear pressure vessel steel, A508CL3, and its joints welded by narrow-gap submerged-arc welding. Int J Press Vessel Pip 76:35–41
3. Verón P, Hippsley CA, Knott JF (1984) Comparative studies of stress-relief cracking in relaxation test specimens and in a full-scale weldment. Int J Press Vessel Pip 16:29–51
4. Hurrell, PR, Pellereau BME, Gill CM, Kingston E, Smith D, Bouchard PJ (2014) Development of residual stress profiles for defect tolerance assessments of thick section electron beam welds, in Proceedings of the ASME 2014 Pressure Vessels and Piping Conference, Anaheim, USA, 1–12
5. Li K, Lu FG, Cui HC, Li XB, Tang XH, Li ZG (2015) Investigation on the effects of shielding gas on porosity in fiber laser welding of T-joint steels. Int J Adv Manuf Technol 77:1881–1888
6. Assunção E, Quintino L, Miranda R (2010) Comparative study of laser welding in tailor blanks for the automotive industry. Int J Adv Manuf Technol 49:123–131
7. Yoon SH, Hwang JR, Na SJ (2007) A study on the plasma-augmented laser welding for small-diameter STS tubes. Int J Adv Manuf Technol 32:1134–1143
8. Li SC, Chen GY, Zhou C (2015) Effects of welding parameters on weld geometry during high-power laser welding of thick plate. Int J Adv Manuf Technol 79:177–182
9. Riahi M, Amini A (2013) Effect of different combinations of tailor-welded blank coupled with change in weld location on mechanical properties by laser welding. Int J Adv Manuf Technol 67:1937–1945
10. Jones LP, Aubert P, Avilov V, Coste F, Daenner W, Jokine T, Nightingale KR, Wykes M (2003) Towards advanced

welding methods for the ITER vacuum vessel sectors. Fusion Eng Des 69:215–220
11. Zhang XD, Ashida E, Tarasawa S, Anma Y, Okada M, Katayama S, Mizutani M (2011) Welding of thick stainless steel plates up to 50 mm with high brightness lasers. J Laser Appl 23(022002):1–8
12. Elmesalamy A, Francis JA, Li L (2014) A comparison of residual stresses in multi pass narrow gap laser welds and gas-tungsten arc welds in AISI 316L stainless steel. Int J Press Vessel Pip 113:49–59
13. Guo W, Dong SY, Guo W, Francis JA, Li L (2015) Microstructure and mechanical characteristics of a laser welded joint in SA508 nuclear pressure vessel steel. Mater Sci Eng A 625:65–80
14. Elmesalamy AS, Li L, Francis JA, Sezer HK (2013) Understanding the process parameter interactions in multiple-pass ultra-narrow-gap laser welding of thick-section stainless steels. Int J Adv Manuf Technol 68:1–17
15. Yu YC, Yang SL, Yin Y, Wang CM, Hu XY, Meng XX, Yu SF (2014) Multi-pass laser welding of thick plate with filler wire by using a narrow gap joint configuration. J Mech Sci Technol 27: 2125–2131
16. Zhou Z, Wu W, Wei J, Du S, Han S, Liu L, Yu X, Li H, Foussat A, Libeyre P (2012) Research on manufacture and enclosure welding of ITER correction coils cases. IEEE Trans Appl Supercond 22: 4202603
17. Jokinen T, Kujanpa¨a¨ V (2003) High power Nd:YAG laser welding in manufacturing of vacuum vessel of fusion reactor. Fusion Eng Des 69:349–353
18. Cox TB, Low JR (1974) An investigation of the plastic fracture of AISI 4340 and 18 Nickel-200 grade maraging steels. Metall Trans 5:1457–1470
19. He Y, Yang K, Sha W (2005) Microstructure and mechanical properties of a 2000 MPa grade Co-free maraging steel. Metall Mater Trans A 36:2273–2287
20. Valiev RZ, Langdon TG (2006) Principles of equal-channel angular pressing as a processing tool for grain refinement. Prog Mater Sci 51:881–981
21. Masumura R, Hazzledine P, Pande C (1998) Yield stress of fine grained materials. Acta Mater 46:4527–4534